

Towards Glioma Intra-operative Photodynamic Therapy: Targeted Photo-active Nanoparticles in a Brain Tumor Window Model

Kristen A Simmer¹, Hoe Jin Hah¹, Yong-Eun Koo Lee¹, Oren Sagher², Daniel Orringer², Martin Philbert³ and Raoul Kopelman^{1,*}

¹Department of Chemistry, University of Michigan, Ann Arbor, MI, USA

²Department of Neurosurgery, University of Michigan, Ann Arbor, MI, USA

³Toxicology Program, University of Michigan, Ann Arbor, MI, USA

*Corresponding author: Raoul Kopelman, Department of Chemistry, University of Michigan, Ann Arbor, MI, USA, E-mail: kopelman@umich.edu

Received date: 29 October 2015; Accepted date: 6 Nov 2015; Published date: 10 Nov 2015.

Citation: Simmer KA, Hah HJ, Lee Y-E K, Sagher O, Orringer D, et al. (2015) Towards Glioma Intra-operative Photodynamic Therapy: Targeted Photo-active Nanoparticles in a Brain Tumor Window Model. *Int J Nanomed Nanosurg* 1(2): doi <http://dx.doi.org/10.16966/2470-3206.106>

Copyright: © 2015 Simmer KA, et al. This is an open-access article distributed under the terms of the Creative Commons Attribution License, which permits unrestricted use, distribution, and reproduction in any medium, provided the original author and source are credited.

Abstract

We present the development and characterization of Methylene-Blue-loaded nanoparticles (MB-NP) as well as their phototherapeutic application in an *in vivo* rat glioma model. The photo sensitizer, Methylene-Blue was covalently conjugated to the nanoparticle matrix to prevent the potential for leaching and non-specific staining of target and ancillary tissues. *In vitro* experiments demonstrate high efficiency in producing reactive oxygen species (ROS) and concomitant cytotoxicity. *In vivo* experiments were performed by first optimizing therapeutic parameters such as nanoparticle surface modification by attachment of F3-peptide targeting moieties, dose/concentration administered, incubation time, light-fluence and time of illumination. The quantitative growth patterns of the glioma were determined through visual observation of the tumorigenic response to various treatment parameters, using a cranial window model *in vivo*. The cranial window permitted non-invasive external illumination of the tumor and evaluation of loading of tumors with nanoparticles, the effects of particle targeting on retention *in situ*, and efficacy. The targeted MB-NP produced significant delay in tumor growth compared to control groups, demonstrating some potential advantages of nanoparticle-based PDT and its promise for the rapid eradication of local tumors. Furthermore, this approach holds promise as a potential surgical adjuvant palliation of any remaining tumor mass.

Keywords: Glioma; Photodynamic therapy; Photo-active nanoparticles; Brain tumor

Introduction

Primary malignant brain tumors and especially Glioblastoma multiforma represent one of the most formidable challenges facing oncologists today. The propensity of these tumors to infiltrate normal, functioning brain complicates regional treatments like surgery and radiation therapy. Moreover, the relative resistance of the tumor cells to cytotoxic agents and difficulty in delivery of these agents across the blood brain barrier hamper efforts to kill individual tumor cells [1-3]. These tumors, once discovered, inexorably progress, ultimately causing death, usually less than two years after diagnosis [1].

Against this backdrop of apparent futility, there have been promising recent advances in the treatment of malignant gliomas. Recent discovery of defects in the genetic makeup of certain malignant gliomas has identified a subset of tumors that respond well to treatment with certain chemotherapeutic agents [2]. In addition, converging lines of evidence suggest that maximal surgical removal of the tumor affords a survival advantage. Immunological therapies such as dendritic cell vaccines have also surfaced, although these modalities are still in early phase studies. So far, all these approaches remain promises for a not yet achieved rosier future.

The resurgence of surgery as a viable therapy for malignant gliomas has refocused clinicians and scientists on the potential advantages and disadvantages of this approach. The advantages of cytoreduction have already been demonstrated, but there are obvious limits to them. Direct access to the tumor at the time of surgery also allows surgeons to deliver “non-surgical” treatments to the tumor bed. The development of Gliadel as an adjuvant treatment delivered at the time of surgery was an early

attempt to leverage the operating room for delivery of nonsurgical therapy; and while the efficacy of Gliadel was limited by the relatively limited efficacy of the chemotherapeutic agent Carmustine, the concept of direct treatment of the tumor in the operating room still holds promise [3]. The path we have chosen, photodynamic treatment (PDT), has the simplicity of merely shining (laser) light on the tumor bed at the conclusion of the surgical resection, provided that cell specific targeting has been achieved, i.e., the photo drug has been selectively taken up by the tumor cells [4-49]. We report below on a study that simulates intraoperative PDT, using a rat brain window model.

Regarding PDT, choice of a suitable photosensitizer is of the utmost importance when designing a PDT agent. The ideal agent should exhibit chemical purity, nominal dark toxicity for the photosensitizer and its metabolites, high efficiency of tumor selectivity, high photochemical ability, activation, i.e., absorbance at long wavelengths, within the therapeutic window (600-900 nm), enabling sufficient tissue penetration, as well as rapid system clearance to diminish photosensitivity [4-8]. The above requirements, and especially the consequences of skin phototoxicity, led to second generation photosensitizers. Second-generation synthetic photosensitizers are recognized for having known chemical composition, a greater affinity for tumor selectivity, shorter periods of photosensitivity, higher yields of singlet oxygen, and an increase in penetration depth due to their longer activation wavelengths [9]. Regarding our choice of Methylene Blue (MB), it is a second-generation photosensitizer with well-established photochemical properties, including a high quantum yield of singlet oxygen generation ($\Phi_{\Delta} \sim 0.5$), and has been established as a highly efficient sensitizer for PDT [10]. Methylene Blue belongs to the phenothiazinium family, allowing for increased efficacies of singlet

oxygen production and a high molar absorption coefficient ($\epsilon_{\max} \sim 82,000 \text{ M}^{-1} \text{ cm}^{-1}$). Furthermore, this dye has excitation within the therapeutic window (600-900 nm), allowing for greater penetration depths [6,11-16]. Methylene Blue has been used for a number of medical applications and therapies [17-23]. By 2013, over 13,000 entries for “Methylene Blue” have been accepted by the biomedical library PubMed. Methylene Blue has been used as a histochemical stain, a biochemical reagent and a chief compound in the development of therapeutic agents for diseases ranging from microbial infections to cyanide poisoning, and from Malaria to Alzheimer’s disease [18-23]. There have been extensive experimental studies considering the application of Methylene Blue for photodynamic therapy *in vitro* [6,24], *in vivo* [25] and in clinical studies [7,26-29], and it has been identified as having a promising potential for the treatment of cancer. Clinical PDT treatments and trials using Methylene Blue include basal cell carcinoma, melanoma, Kaposi’s sarcoma [30], and chronic periodontitis [31]. However, the widespread use of Methylene Blue as a photosensitizer for clinical PDT has been limited due to its susceptibility to enzymatic degradation when delivered intravenously. Notably, Methylene Blue can easily cross the cell membrane and anchor in the mitochondria [32,33], lysosomes [34] and double-stranded DNA [35]. It has been found that when Methylene Blue binds to the mitochondria it can traverse the matrix by the mitochondrial matrix proton potential [32]. Additionally, an increase in local concentrations of Methylene Blue induces the formation of Methylene Blue dimers, previously shown to be less effective in production of reactive oxygen species [11,12]. Such accumulation of Methylene Blue in cellular organelles, as well as in serum, reduces the compound by oxidation to the colorless Leuko-Methylene Blue (LMB), a molecule with no photodynamic ability [15,25,26]. Examples of uptake and reduction of Methylene Blue have been attributed to both the thiazine dye reductase found on the surface of endothelial cells and to NADH/NADPH within cells [36-38].

The ability to maintain the photosensitizing capability of Methylene Blue in a biological environment is critical for its application to PDT of cancer. Its incorporation into a nanoparticle matrix composed of polymers such as polyacrylamide (PAA), silica, or poly (lactic-co-glycolic acid), can serve to embed the active form of the Methylene Blue photosensitizer, protecting it against enzymatic degradation [39]. Furthermore, nanoparticle surface modification can allow for enhanced and selective targeting by attachment of a tumor specific homing moiety, e.g. the F3-peptide, as well as coating it with polyethylene glycol (PEG) for longer plasma circulation time [40].

Loading of the Methylene Blue photosensitizer can be achieved by (1) physical encapsulation during synthesis or (2) post loading after synthesis or (3) by covalently linking the dye to the PAA nanoparticle matrix. The more demanding process of covalently linking the dye pays off by preventing leaching related problems during *in vivo* studies. This loading method has been designed and tested, in a serum solution, in cells, and *in vivo* and has exhibited a good potential for future clinical applications [39].

We note here the many advantages to the use of PEGylated NPs for PDT, due to its ability to (1) reduce systemic toxicity of the drugs, due to tumor targeting, (2) improve the local delivery and specificity of drugs, as well as (3) enhance its plasma circulation time [41-49]. Engineering the nanoparticles to be within the desired diameter, of 10-100 nm, avoids renal elimination and recognition by phagocytes [41-43]. Nanoparticle accumulation in the brain tumor tissue, and vasculature, is achieved through the “enhanced permeability and retention effect” (EPR), allowing macromolecules and NP’s retention within the tissue by way of a leaky microvasculature and poor lymphatic drainage [44-49]. Nanoparticle matrix surface engineering can further improve the retention time within the tumor tissue by the attachment of a tumor specific homing moiety, e.g. the F3-peptide; it also enhances the plasma circulation time

(~24 hours) by coating the matrix with polyethylene glycol (PEG) [43]. These novel NP delivery methods minimize side effects as well, and thus enhance the therapeutic efficiency. To avoid possible side effects caused by the accumulation of nanoparticles post-treatment, biodegradable cross-linkers are incorporated into the nanoparticle matrix, allowing for slow bio-degradation and bio-elimination *in vivo* [48].

Polyacrylamide nanoparticles containing the PDT agent Photofrin, surface-modified with F3-peptide, have been utilized for specific targeting of gliosarcoma cells; the nanoparticle targeting has displayed high intratumoral NP uptake, thereby increasing the photo toxicity, resulting in complete remission of tumor for 40% of the animals treated with F3-targeted Photofrin nanoparticles, while, on the other hand, all control rats, including those treated with non-targeted NPs or free Photofrin, died within 2 weeks [48,49].

In the present work, the photosensitizer Methylene Blue was covalently conjugated to the nanoparticle matrix and used in both *in vitro* and *in vivo* experiments to test its proficiency in producing reactive oxygen species as well as its cell killing ability. The *in vivo* experiments utilized glioma bearing rats adorned with cranial windows, allowing for direct serial inspection of various therapy parameters, such as nanoparticle dose, effect of surface modification by attachment of F3-peptide targeting moieties, incubation time and light fluence. These windows allowed the conduction of PDT by an externally placed laser and the evaluation of tumor growth and necrosis, as a function of NP design, such as PEGylation and targeting, as well as of PDT parameters, such as drug dose, NP dose, light dose and timing of illumination.

Experimental

Nanoparticle synthesis

Materials: Methylene Blue succinimidylester (MB-SE) was purchased from Emp. Biotech. Acrylamide (AA), 3-(acryloyloxy)-2-hydroxypropyl methacrylate (AHM), ammonium persulfate (APS), N,N,N’,N’-tetramethylethylenediamine (TEMED), sodium dioctylsulfosuccinate (AOT), Brij 30, were all acquired from Sigma-Aldrich (St Louis, MO). 3-(aminopropyl) methacrylamide hydrochloride salt (APMA) was purchased from Polysciences Inc. (Warrington, PA). Ethanol (95%) and hexane were purchased from Fisher Scientific. Phosphate-buffered solution (PBS) was made using a phosphate-buffered saline tablet from Sigma-Aldrich. F3-Cys peptide (KDEPQRRSARLSAKPAPPKPEPKPKKAPAKKC) was purchased from SynBioSci. The heterobifunctional PEG (MAL-PEG-NHS, 2k) was purchased from Creative PEG Works. All chemicals were used as purchased without further purification.

Preparation of methylene blue nanoparticles: Methylene Blue-conjugated polyacrylamide nanoparticles were prepared by a reverse micro emulsion polymerization method [21]. A monomer solution was prepared by dissolving monomers, acrylamide and biodegradable cross-linker, AHM, in PBS. A dye solution consisting of MB-SE and APMA was prepared and gently stirred for 2 hours at room temperature. The monomer solution and the dye solution were sonicated and added to a deoxygenated hexane solution containing two surfactants, AOT and Brij 30. The two mixtures were emulsified by stirring for 20 min, followed by the initiation of polymerization by addition of a freshly prepared APS solution (10% w/v) and TEMED. The solution was then stirred under inert atmosphere, at room temperature, for 2 hours. After completing the polymerization, hexane was removed using a Rota vapor-P (Brinkmann Instruments) and the residue was suspended in ethanol. Excess surfactant and dye from the remnant mixture were removed by washing the particles with ethanol and distilled water through an Amicon ultra-filtration cell (Millipore Corp., Bedford, MA), with a 300 kDa filter membrane under

pressure (10-20 psi). The resultant nanoparticles were then freeze-dried using a 5 L Modulyo D freeze dryer (Thermo Fisher Scientific).

F3-Peptide conjugation to polyacrylamide nanoparticles: F3-peptides were conjugated to the surface of the nanoparticles for specific targeting to nucleolin expressed on the glioma cells. The freeze-dried PAA nanoparticles (50 mg) were dissolved in PBS (2.5 mL, pH 7.4) and bifunctional PEG (4 mg) was conjugated to the nanoparticle surface by amine-succinimidyl ester. This mixture was allowed to react under stirring condition for 30 min at room temperature before undergoing thorough washings using an Amicon centrifugal filter (Millipore, 100 kDa) thereby removing any unreacted ligands, and the final solution concentrated to ~20 mg/mL. Cystein tagged F3-peptide, F3-Cys peptides (0.06 μ mol), were added to the concentrated nanosensor solution and gently stirred overnight (>6 hours), at room temperature. L-Cysteine aqueous solution was added to the mixture and stirred for 2 hours in order to deactivate the terminal site of unreacted PEG. The resultant F3-targeted MB-conjugated PAA nanoparticle solution was thoroughly washed with PBS and distilled water in an Amicon ultra-filtration cell (Millipore Corp., Bedford, MA), and then freeze-dried with a 5L ModulyoD freeze dryer (Thermo Fisher Scientific) until re-hydrated for experimental use (Figure 1).

Surface modification of non-targeted nanoparticles: Dye-conjugated PAA nanoparticles (50 mg) were dissolved in PBS (2.5 mL, pH 7.4). Bifunctional PEG (4 mg), was added to the nanoparticles solution and then the mixture was stirred for 30 min at room temperature. A rinsing procedure was carried out, using an Amicon centrifugal filter (Millipore, 100 kDa), removing any unreacted ligands, and concentrated to ~20 mg/mL. Following the addition of PEG, an aqueous solution of L-Cysteine was added to the mixture and stirred for 2 hours in order to deactivate the terminal site of PEG. The resultant non-targeted MB-conjugated polyacrylamide nanoparticle solution was thoroughly washed with PBS and distilled water in an Amicon ultra-filtration cell (Millipore Corp., Bedford, MA), and then freeze-dried with a 5 L ModulyoD freeze dryer (Thermo Fisher Scientific) until re-hydrated for experimental use.

Nanoparticle characterization

Dynamic light scattering (DLS) measurements: The size distribution of the MB-conjugated PAA nanoparticles in an aqueous solution was measured by dynamic light scattering (DLS, Delsa Nano, Beckman Coulter, Inc., Brea, CA, USA). The surface charge of the MB-conjugated PAA nanoparticles in water was measured as a zeta potential value, using the above instrument.

Quantification of methylene blue loading: The amount of conjugated Methylene Blue in the nanoparticles was evaluated by absorption measurements, using a UV-Vis spectrometer (UV-1601, Shimadzu, Scientific Instruments Inc., Columbia, MD, USA). The amount of photosensitizer loaded was calculated using a calibration curve constructed from a series of known concentrations of Methylene Blue and the Beer-Lambert law.

Reactive oxygen species detection: ROS (reactive oxygen species) production from MB-PAA NPs was measured using Anthracene-9,10-dipropionic acid disodium salt (ADPA) as a ROS (1O_2) detection probe [50,51]. MB-conjugated nanoparticles were suspended in PBS and mixed with ADPA in a cuvette and while under constant stirring the solution was irradiated at the excitation wavelength to determine 1O_2 generation using fluorescence spectroscopy (FluoroMax-3, Jobin Yvon/SPEX Division, Instruments S.A. Inc., Edison, NJ, USA).

Toxicity analysis

MTT assay: For cytotoxicity studies, 9L glioma cells were plated on 96-well plates, at a density of 5000 cells per well and incubated at 37°C overnight. For comparison, the cells were incubated with blank

PAA, PEGylated PAA, and F3-targeted PAA nanoparticles at various concentrations (0.1, 0.2, 0.5, and 1.0 mg/mL) and left for 2 hours at 37°C with slow intermittent rocking. After incubation, to remove any unbound nanoparticles, the treated cells were carefully washed 3 times with fresh cell medium. The cells were further prepared using the MTT assay kit; 25 μ L of 5.0 mg/mL 3-(4,5-dimethylthiazol-2-yl)-2,5-diphenyltetrazolium bromide (MTT) in PBS was added to each well and left to incubate for 4 hours while slowly rocking. After 4 hours the solution was removed and 200 μ L of DMSO was added to each well, so as to solubilize the water-insoluble formazan crystals produced by the MTT cellular dehydrogenase activity in viable cells. The 96-well plate was covered with foil and left to steadily rock on a 55S single platform shaker (Reliable Scientific, Inc) overnight. To quantify cell viability of the treated cells, the absorbance spectra was analyzed using a micro plate reader (Spectra MAXPlus 384, Molecular Devices LLC, Sunnyvale, CA) at 550 nm and compared to untreated cells. Each condition was performed using 12 wells so as to assure dependable results.

Endotoxin detection: Endotoxin levels were measured using an Endosafe-PTS (Charles River) and following the LAL Assay [52]. A portable endotoxin meter has sterile cartridges for detecting endotoxin in aqueous samples. Within the device, a reaction between horseshoe crab blood extract, limulus amoebocyte lysate (LAL), and bacterial endotoxin or with a membrane component of Gram negative bacteria can quantify bacterial endotoxins. All nanoparticle batches and samples were tested one hour prior to injecting the nanoparticle solution into the animal model during PDT treatment.

Based on our experience with testing endotoxin levels for the nanoparticle samples, bacteria growth rates are highly sensitive to both time and temperature; longer exposure to solutions after hydration and warm temperatures can exacerbate bacteria growth. To avoid growth and contamination, the nanoparticle samples were rehydrated with minimal time intervals between hydration and injection; in addition, the sample was refrigerated at all times post rehydration, with the exception of when the sample was warmed to physiological temperature prior to injection.

Cell culture

Rat 9L gliosarcoma cells (Brain Tumor Research Center, University of California, San Francisco, CA) were routinely maintained in Rosewell Park Memorial Institute medium (RPMI) with 400 mg/L D-glucose and 292 mg/mL L-glutamine supplemented with 10% fetal bovine serum, 100 U/mL (3%) penicillin, 1mM sodium pyruvate, and 100 μ g/mL streptomycin sulfate. Cells were grown at 37°C, 5% CO₂, 95% air, and 100 % humidity environment. Cells were placed on the 96 well plates for the MTT assay and on 35mm culture dishes with cover slip bottom, for *in vitro* PDT.

In vitro studies

Fluence dependent PDT: To investigate the effects of PDT photo toxicity, a series of *in vitro* experiments were performed on rat 9L gliosarcoma cells. Glass cover slips were incubated with 1 mg/mL MB-loaded polyacrylamide nanoparticles (containing F3-peptide) for 1 hour, rinsed with appropriate cell media and placed in a temperature-controlled sample chamber at 37°C. Methylene Blue mediated cytotoxicity was then monitored before and after illumination by labeling the cells with 5 μ L Calcein-AM and 10 μ L propidium iodide (PI) fluorescent stains. Fluorescent observations of Calcein-AM (excitation: 490 nm, emission: 515 nm) and PI (excitation: 536 nm, emission: 617 nm) were monitored for 30 minutes using a Perkin Elmer Ultra View Confocal microscope system equipped with an argon-krypton laser. Irradiation with the microscope laser illumination was performed at 671 nm, for 1-minute intervals and stopped. The live/dead assay allows for obvious distinctions

of viable/cytotoxic cells. In living cells, intracellular esterase converts the non-fluorescent Calcein-AM into a green fluorescent Calcein, indicating a viable cell. PI is barred by viable cells but can invade cells with damaged membranes. Upon irradiation, in a time-dependent manner, compromised cells release the green fluorescence of the Calcein-AM through damaged membranes and permit the binding of PI to their nucleic acids - emitting red fluorescence. A series of images of the cells were sequentially taken for 30 minutes, in minute intervals, using an Olympus IX-70 confocal microscope. Upon completion of exposure, the objective was switched to a lower magnification so as to show that the treatment was localized to the illumination area - showing red stained, dead cells, which are surrounded by viable, green stained cells, just outside the illuminated area. At each time interval, the survival rate was presented as a percentage of the number of viable cells divided by the total number of cells (viable and non-viable).

Furthermore, separate fluency-dependent PDT studies were performed at an illumination power density of 100 mW/cm² and 222 mW/cm². Pre-exposure images were taken using a 60X objective. The cells were exposed, for a total of 30 minutes, to a 671 nm red diode laser (model 671RLMH1W, Changchun Dragon Lasers Co., Ltd) with light intensity of 100 mW/cm² and 222 mW/cm². Post-exposure images were taken using a 20X objective, to observe the localized cellular damage.

In vivo studies

Cranial window model

The animal research protocol was reviewed and approved by the University Committee on Use and Care of Animals (UCUCA) at the University of Michigan, Ann Arbor. Biparietal craniectomies were performed on 8-week old Sprague-Dawley male rats (Charles River Laboratory, Wilmington, MA). Rats weighing between 250 to 350 g were anesthetized and placed into a stereotactic frame. Rat 9L gliosarcoma cells were harvested in monolayers and following a full craniectomy suspended in media and the cells (10⁵) were injected using a syringe micro-injector (Med fusion 3500 syringe pump). The 9 L cells were implanted in the forebrain at a depth of 1.5 mm through a burr hole extending 1 mm below the injection location to create a pocket for growth. To allow for serial inspection, a thin, round microscope cover slip was bonded to the cranial opening with cyanoacrylate glue creating a brain tumor window (BTW) model [53].

Methylene Blue nanoparticle administration: The Methylene Blue conjugated nanoparticles had a dye loading efficiency of 0.27% wt/(NP wt) and the dose administered was equivalent to 0.86 mg of MB/(kg of rat). The stock solution was determined to have nominal endotoxin levels as determined by the LAL assay. Once the tumor radius reached 2-3 mm in diameter, photosensitizers in the form of free dye, or embedded within polyacrylamide nanoparticles, were administered intravenously through the right femoral vein using a programmable micro-injector (Med fusion 3500 syringe pump). After injection, rats were kept in the dark until undergoing irradiation therapy.

Illumination parameters: Tumors in the BTW model were irradiated in a cross sectional manner, via the exposed tumor surface immediately beneath the window. *In vivo* light illumination was performed using a 671 nm red diode laser (model 671RLMH 1 W, Changchun Dragon Lasers Co., Ltd) with tunable output power (0-1 W), to precisely expose at various fluency rates.

A CSMA-8-B collimator (Newport Corp) was used to control the radius of the laser beam (and hence fluence rates). For all experiments, a constant beam diameter of 4 mm was maintained, at a constant distance of 1 inch (metric conversion in mm) between the cranial window and the collimator. The laser was calibrated by warming at X joules/power-setting for 30 minutes, and the beam measured with a XX power meter to assess beam stability during a period of no less than 1 hour.

Measurement of tumor surface area: Damage to sensitized tumor and brain parenchyma by photo irradiation was observed using a Sony digital camera. Daily photographs of the cortical surface through the BTW provided an evident depiction of the tumor growth patterns prior and post PDT treatments. Tumor growth patterns were then evaluated by delineating the tumor boundaries, based on the variations of pixelated coloration and measuring the total pixelated surface area of the tumor. The *in vivo* PDT efficiency was determined by measuring tumor surface area as seen through the BTW and comparing tumor growth patterns of individual animals and animal groups. Surface area dimensions were taken by quantifying tumor tissue remaining post-irradiation and normalizing to the tumor area measured on PDT-treatment day (day 0). Post-treatment areas of necrotic tissue were recorded. We emphasize that tumor growth patterns were calculated by measuring the surface area of the tumor tissue as seen through the BTW

Results and Discussion

The size of the surface-modified Methylene Blue-conjugated polyacrylamide nanoparticles, measured using the DLS data, indicated that the mean diameter of the modified nanoparticles in solution was 55.0 (± 5.0) nm (Figure 2), and was similar to that of the unmodified nanoparticles. Thus modification of the surface by the attachment of PEG, and/or by targeting ligands, had no significant effect on the size of particles in solution. These nanoparticles fall within the optimal range of 10-100 nm which has proved to be very effective for *in vivo* applications; this is because nanoparticles greater than 10 nm have the ability to avoid clearance by the kidney, allowing for prolonged and elevated circulatory levels, and nanoparticles smaller than 100 nm avoid entrapment by phagocytes [54-55]. Furthermore, leaky angiogenic vasculatures have fenestrations, which improves the penetration phenomenon of the enhanced penetration and retention (EPR) effect, allowing nanoparticles to be delivered and to accumulate in tumor tissue, more readily than in the surrounding healthy tissue [44-47,56].

The F3-modified nanoparticles have a surface charge of +12 (± 1) mV, whereas the non-targeted (surface PEGylated) nanoparticles have a charge of + 2 (± 1) mV, in comparison to the unmodified nanoparticles that have free amine groups on the surface, having a charge of +14 (± 3) mV. The non-targeted nanoparticles have a near neutral surface charge, due to the presence of the neutral PEG molecules on the particle surface. However, the F3-targeted Methylene Blue-conjugated polyacrylamide nanoparticles display a positive surface charge, because the cationic F3-peptide on the surface of the PEG surface layer of the nanoparticle has a high positive charge.

The amount of covalently linked Methylene Blue in the nanoparticle was determined to be 0.27% by weight [57].

The efficiency of photodynamic therapy depends directly on the ability of the photosensitizer to produce reactive oxygen species (ROS), on the availability of molecular oxygen, on the light fluency (intensity and duration), and on the photosensitizer concentration at the treatment area. Figures 2B and 2C shows the generation of ROS of Methylene Blue dye and Methylene Blue conjugated nanoparticles, using the ADPA method [39, 50]. The ROS production rate constant was measured by the fluorescence decay of ADPA (anthracene-9, 10-dipropionic acid) and was found to be 5.5 × 10⁻⁴/s for 1.0 μM free Methylene Blue dye in PBS. For Methylene Blue 0.37% wt/(NP wt) conjugated nanoparticles the rate constant was 4.35 × 10⁻⁴/s. The capability of the targeted nanoparticles to produce reactive oxygen species and kill cells was optimized through *in vitro* experiments [39]. The latter can provide a foundation of preliminary studies for the *in vivo* PDT protocols: nanoparticle delivery conditions, dose and optimal light fluence vs rudimentary glioma growth rates [39,53].

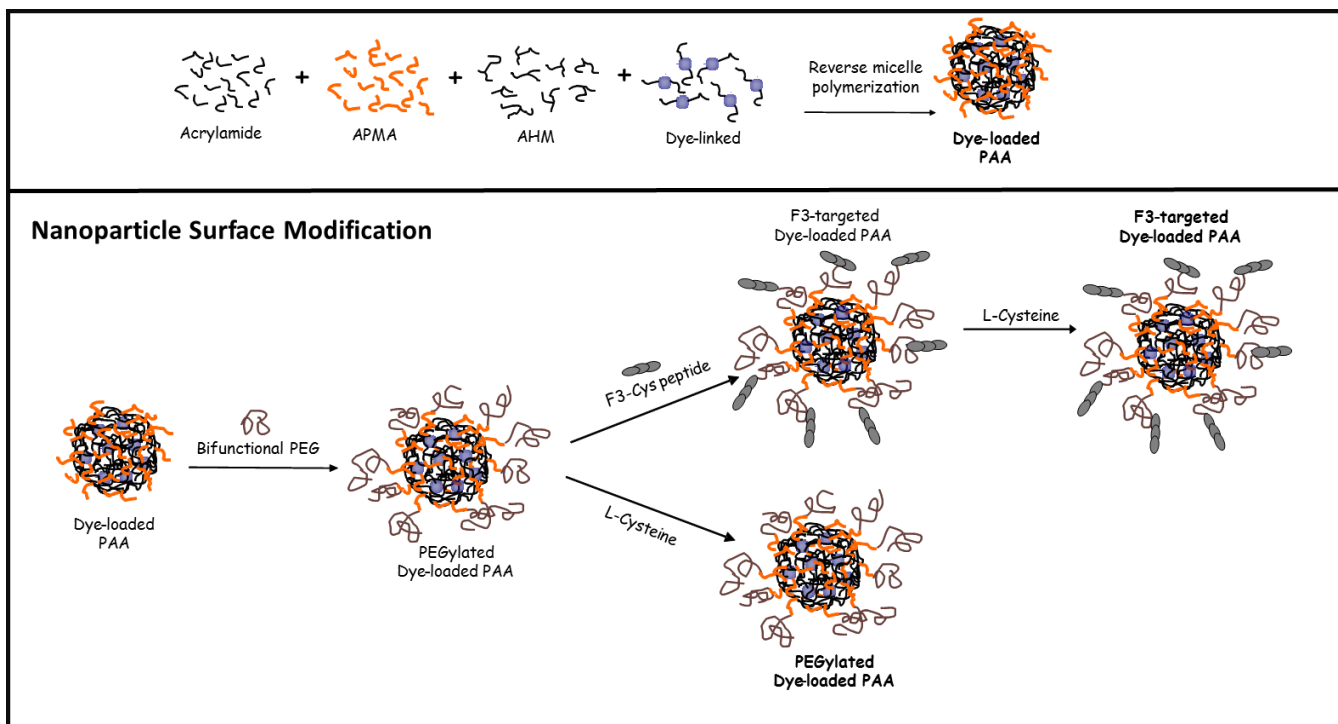


Figure 1: Surface modification and conjugation of MB-loaded PAA nanoparticles

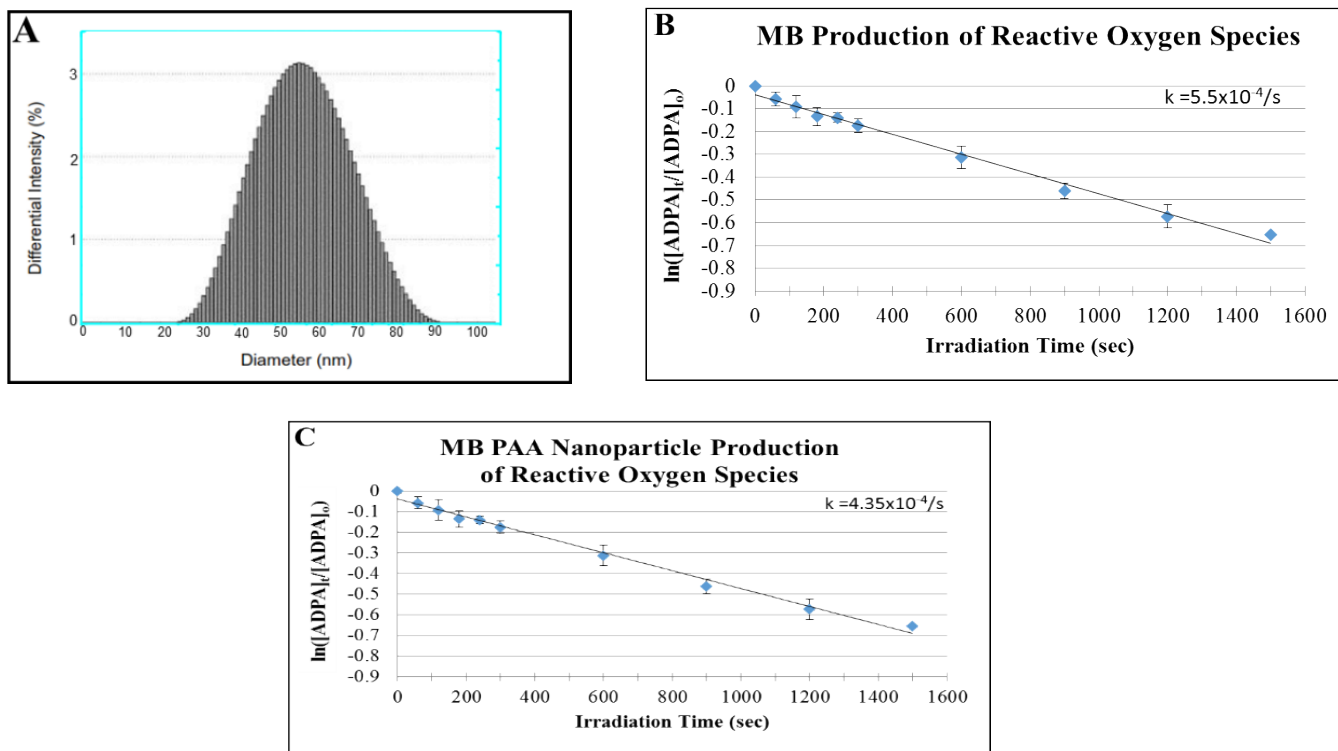


Figure 2: (A) Size distribution of polyacrylamide nanoparticles in solution using dynamic light scattering measurements. ROS production measurement of (B) Methylene Blue free dye in DI water and (C) Methylene Blue polyacrylamide nanoparticles. Peak excitation for Methylene Blue was found at 678 nm: linear fitted plot of fluorescence change in ADPA as a function of irradiation time.

To investigate the dark toxicity, as well as PDT efficacy, of Methylene Blue-conjugated polyacrylamide nanoparticles in the *in vitro* experiments, MTT assays were carried out for various doses of the nanoparticles. F3-targeted and non-targeted nanoparticles were added with increasing concentrations for survival assessment as determined by the MTT assay. The cytotoxicity of the nanoparticles was determined by the conversion of MTT to formazan via mitochondrial oxidation. Cell survival rates showed no significant differences among cells treated with Methylene Blue polyacrylamide nanoparticles (in the dark) and the control (cells only). The average cell survival rates exhibited a higher than 97% viability, up to 1mg/ml nanoparticle concentration (Figure 3). Overall, the treated cells endured no detectable cytotoxicity as a result of being treated with the Methylene Blue polyacrylamide nanoparticle solution (in the dark), ensuring that viability variances in PDT experiments will not be compromised by dark toxicity produced by the nanoparticles.

It is imperative to test dye leaching because photosensitizers outside the nanoparticle can interact with cellular surface proteins and organelles *in vitro*; furthermore, enzymatic degradation of the leached out Methylene Blue dye might alter the optical properties and photo activity of the dye during intraoperative *in vivo* applications. In order to survey the dye leaching, the Methylene Blue content in the filtrate separated from the nanoparticles by centrifugation filtration was measured, using UV-Vis absorbance spectra [39]. There was no detectable absorbance at 668 nm, verifying negligible dye leaching of Methylene Blue out of the Methylene Blue polyacrylamide nanoparticles. This verifies that the detected reaction between the Methylene Blue dye and the ROS must occur within the nanoparticle. It also verifies that covalently linking the Methylene Blue dye to the nanoparticle matrix completely eliminates dye leaching [39], thus ensuring the delivery of the full pay-load of photo sensitizer to cells *in vitro* or to tumor sites *in vivo*.

To investigate the fluence rate dependence of PDT photo-toxicity, a series of *in vitro* experiments were performed on rat 9L gliosarcoma cells. Using the live/dead assay, 9L cells were irradiated at two separate light intensities, 100 mW/cm² and 222 mW/cm², using an excitation wavelength of 671 nm. A series of images of the cells were sequentially taken over 30 minutes, in 1 minute intervals, using an Ultra-View confocal microscope (Figure 4).

Two experiments were carried out with the intention of examining cytotoxicity rates at different laser fluencies; their images are displayed side-by-side (100 mW/cm²: Figures 4a-4e; 222 mW/cm²: Figures 4f-4j). Before

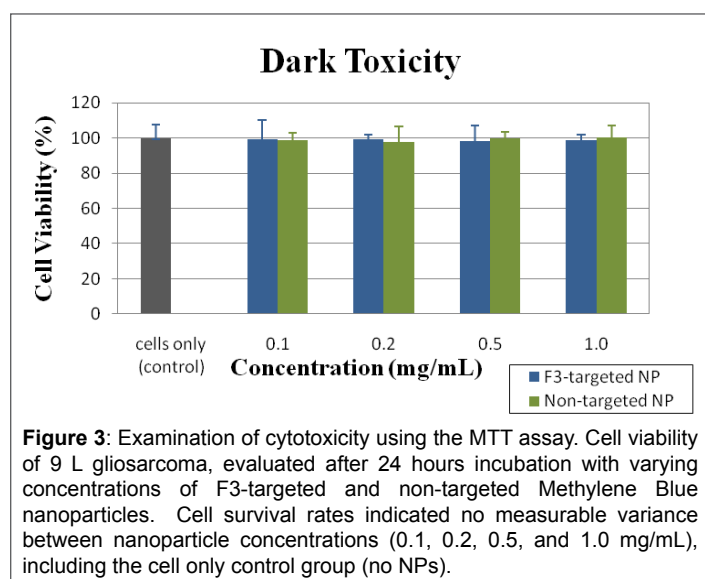
light irradiation, all cells were stained by Calcein-AM, showing green fluorescence, verifying cell viability for both experiments (Figures 4a and 4f). After 5 minutes of irradiation, the cells exposed to the greater fluence rate show the earliest indication of cell death, by the presence of PI-stained red nuclei (Figure 4g) while the cells exposed to the lesser fluence rate show no sign of cellular death (Figure 4b). After completing 10 minutes of illumination, the cells exposed to the higher illumination fluence show a convincing display of cellular death (Figure 4h) and continuously display increasing cytotoxic effects throughout the 30 minute experiment (Figure 4j). Similarly, those exposed to the lower fluence rate displayed primary signs of cell death at 10 minutes and the cellular cytotoxicity intensified between 20 and 30 minutes of illumination (Figures 4d and 4e).

Although the composite confocal images may seem to qualitatively display similar cytotoxic abilities for both experiments, a quantitative analysis displayed a more refined picture of cytotoxicity on the treated cells (Figure 5). This cell viability experiment indicates that a higher fluence rate of laser light has the ability to achieve a faster rate of cellular cytotoxicity, however nearly all cells were killed after 15 min of irradiation with the above given dose.

From the above, one observes that cells exposed to a higher fluence rate display a significantly increased rate of cellular damage, which is induced within a shorter time frame; this was all signified by a rapid release of Calcein-AM (green) through the compromised cellular membrane, allowing for the incorporation of PI (red) into the nucleus. These results demonstrate the light- dose dependency of PDT cytotoxicity, thus indicating that further optimization of the exposure time and fluence rate could enhance the PDT efficacy.

Activation of the photosensitizer in the presence of oxygen is highly cytotoxic, however the short lifetimes (<0.04 μs) and the short diffusion distances (<0.02 μm) of the ROS allow the treatment to be restricted to the nearby cells, tissue and vasculature where the illuminated photosensitizers are present [58]. To further demonstrate the localization and specificity achieved using this localized PDT therapy, a small section of the cells were irradiated using a 60X objective and then the images were captured post-irradiation, using a lower magnification objective, with the irradiated area on the right side of the image (Figures 6c and 6f). The focused illumination induced cell death only to the cells within proximity to the laser beam; whereas adjacent cells, containing methylene blue nanoparticles but not irradiated, display no detectable loss of membrane integrity, as indicated by their green fluorescence. In addition to these localization tests, cells not treated with Methylene Blue-linked polyacrylamide nanoparticle showed no detectable cytotoxicity when exposed to laser irradiation for 30 minutes, at varying fluence rates, suggesting that solely illuminating the cells is not cytotoxic to these cancer cells.

When performing localized PDT *in vivo*, the efficacy of singlet oxygen generation and tumor eradication is directly proportional to the intratumoral concentration of the nanoparticles containing the photosensitizing agent. In order to improve therapeutic efficacy of this treatment it is imperative to understand the kinetics of the targeted nanoparticle, more specifically the incubation time needed to permit the highest concentration of NP at a specific site. Trans-vascular transport and accumulation of the nanoparticles within the glioma domain can be confirmed *in vivo* through delineation experiments. By performing intravital staining experiments, using contrast dye containing nanoparticles for delineation of the implanted neoplasm, direct observation of color variations following the intravenous injection of dye enhanced polyacrylamide nanoparticles can be visualized through the rat cranial window model. Subsequently, this visualization will quantify the optimal irradiation time for the incubation time with greatest accumulation of nanoparticles.



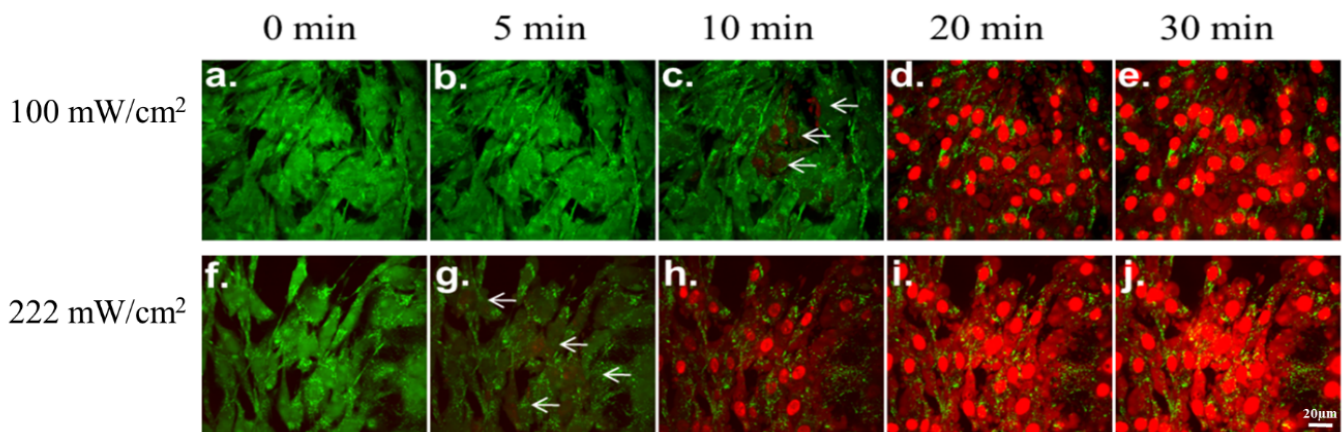


Figure 4: Confocal images of 9L cell lines treated with Methylene Blue-conjugated PAA nanoparticles: Intensity dependent cytotoxicity, induced by F3-targeted Methylene Blue PAA nanoparticles and laser irradiation. The 9L gliosarcoma cells were incubated with Methylene Blue nanoparticles and irradiated with fluencies of 100 mW/cm² and 222 mW/cm². Images were taken (a) before light exposure; (b-e) over 30 min of light exposure at a dose of 100 mW/cm². Images were taken (f) before light exposure; (g-j) over 30 min light exposure at a dose of 222 mW/cm². Cytotoxicity was monitored by labeling the cells with Calcein-AM (green, for viable cells) and propidium iodide (red, for dead cells). Measurements are taken on a confocal microscope.

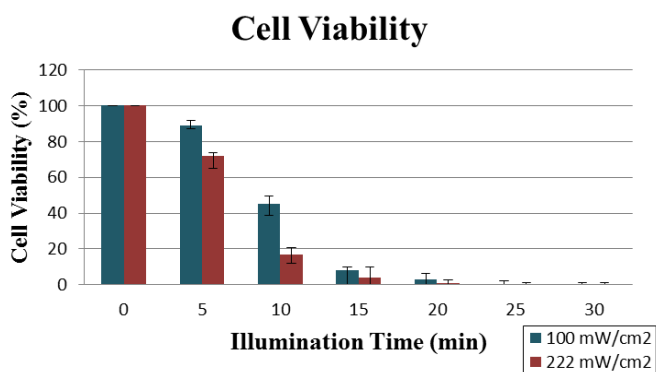


Figure 5: Cell viability assessment for the phototoxic effects of F3-targeted Methylene Blue polyacrylamide nanoparticles on a 9L cell line. Fluency dependent PDT efficiency at light doses of 100 mW/cm² and 222 mW/cm², over the course of 30 minutes of illumination. Cells exposed to a higher fluency responded with a more rapid cellular death than for a lower fluency.

Brain tumor margins are poorly defined when looking through the BTW model. In previous studies, our group performed tumor delineation studies using targeted Coomassie Brilliant Blue (CB) loaded polyacrylamide nanoparticles [59]. Coomassie Blue is an intensely blue colored dye agent and when covalently linked to the polyacrylamide nanoparticles it can be used as a color contrast agent to aid in intraoperative tumor margin delineation. After intravenous injection of the Coomassie Blue polyacrylamide nanoparticles into each rat's femoral vein, the amount of nanoparticles bound to the glioma tissue can be monitored *in vivo*, on a microscopic level, through the rat cranial window model. A quantitative evaluation of tumor delineation resulting from free Coomassie Blue dye, non-targeted CB-linked nanoparticles, and F3-targeted CB-linked nanoparticles, was performed using a Coomassie Blue dose of 35 mg/kg (NP dose was 500 mg/kg). Each treatment resulted in rapid brain tumor delineation, with a more significant color contrast resulting from the use of targeted nanoparticles- a well defined tumor area and strong visual contrast over long time durations.

This delineation study performed by the Kopelman and Sagher labs [53,59] is applicable to determining the optimal times between the

administration of the drug (Methylene Blue, in the form of free dye and encapsulated in nanoparticles) and the illumination time. Determining peak accumulation of Coomassie Blue (CB) nanoparticles within the brain tumor tissue will give insight as to the possible biodistribution of Methylene Blue nanoparticles in the tumor tissue when used for PDT treatment. The Coomassie Blue delineation study revealed peak accumulation of Coomassie Blue free dye at 30 minutes, vs. 120 minutes for non-targeted CB-linked NP-treated animals, while the color contrast for the F3-targeted Coomassie Blue nanoparticles continued to intensify throughout the end of the six-hour experiment. The contrast intensification over time induced by F3-targeted nanoparticles, compared to non-targeted NPs, may be due to the active targeting of the F3-peptide, i.e. their interactions with the nucleolin receptors which are highly expressed on 9 L glioma cells and on the angiogenic vasculature [53-54].

When the brain tumor radius reached 3 mm in diameter, photosensitizers in the form of free dye and dye embedded within polyacrylamide nanoparticles were administered intravenously via the femoral vein. The Methylene Blue-conjugated nanoparticles were administered at a dose of 300 mg/kg, which corresponds to a dose of 0.86 mg MB/kg. This dose has proved to be safe in accordance with previous nanoparticle optimization and toxicology studies [53, 59]. The time interval between nanoparticle administration and light illumination was set at 105 minutes, based on the Coomassie Blue delineation studies performed in the Sagher and Kopelman labs [53,59], concluding that maximal accumulation of both targeted and non-targeted nanoparticles occurs at 120 minutes post-injection [53]. To guarantee light exposure during this maximal accumulation of nanoparticles within the brain tumor, laser illumination was started at 105 minutes post-nanoparticle injection and preceded for 30 minutes, ensuring that irradiation occurred 15 minutes before and after the optimal irradiation window. The light dose was fixed at 180 J/cm² [53]. To monitor tumor growth patterns, daily photographs of the cortical surface through the BTW on the rat model, prior and post PDT treatments, were taken (Figure 7).

A systemic incubation time of 24 hours was also selected to further explore the consequence of incubation time on the PDT effects on tumor growth patterns. The goal of this work was to establish defined incubation conditions for use in future PDT experiments and to optimize predictive functions of the exposure. The time interval of 24 hours between nanoparticle administration and light illumination was based on previous

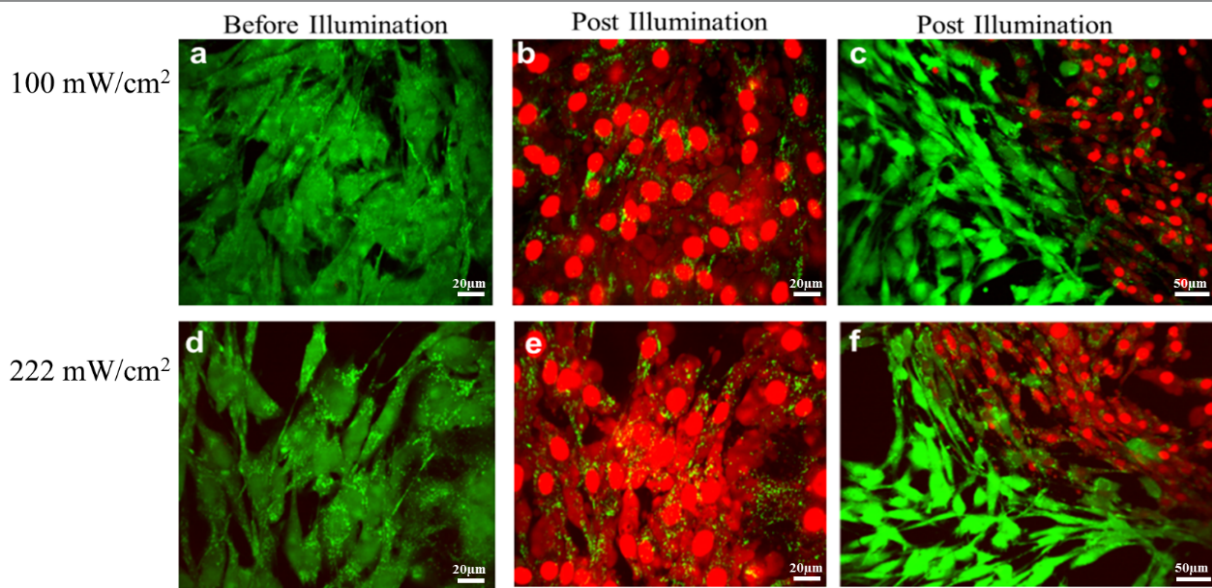


Figure 6: Confocal images of 9L cell lines treated with Methylene Blue-conjugated PAA nanoparticles, before and after laser illumination. Cell viability was monitored by labeling cells with Calcein-AM (green, viable cells) and propidium iodide (red, dead cells). Images were taken before illumination at 60X magnification (a,d), showing no cell death. Post-illumination images were taken at 60x (b,e), illustrating cell death, and were also taken at a lower magnification (c,f) to illustrate that cellular death merely occurred in the area exposed to laser irradiation.

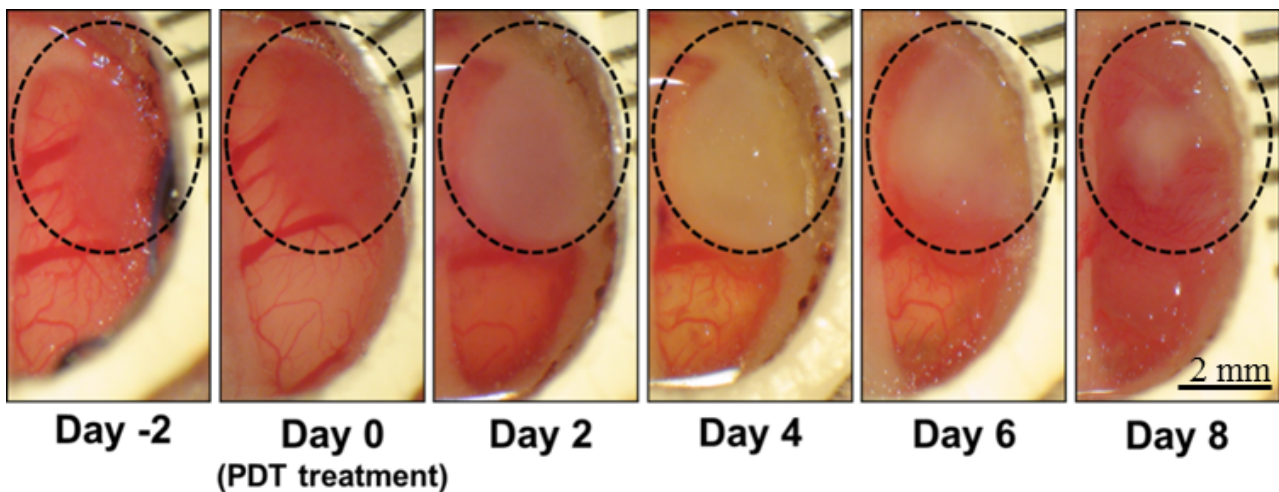


Figure 7: A series of cranial window pictures of a rat with an implanted 9L glioma, before and after the PDT, using F3-Methylene Blue polyacrylamide nanoparticles and a time interval of 105min between nanoparticle injection and light illumination. The dotted circle encloses the tumor area in each picture.

studies using HPPH post-loaded polyacrylamide nanoparticles on mice bearing Colon 26 tumors [60].

The tumor growth curve (Figures 9 and 10) demonstrates that, for equivalent protocols with varying incubation times, the PDT protocol with 105-minute incubation was more effective at inducing photo-toxicity than the one with incubation of 24 hrs. Retardation in tumor growth was evident six days post-treatment, and significantly noticeable differences in tumor size were seen through day ten. Thus, irradiation performed at 105 minutes post-drug injection resulted in a more favorable treatment outcome when compared to the 24 hour incubation.

Evaluation of the effects of different treatments on the tumor growth patterns was accomplished and is presented in Figure 10. Control animals

were not injected with photosensitizer, nor were they exposed to laser light; this group was purely acting as a control group for determining tumor growth patterns post tumor implantation surgery. Animals treated with laser illumination and free photosensitizer were dosed with 0.86 mg/kg of the Methylene Blue free dye and the effect on tumor tissue was assessed after 105 minutes of systemic incubation of the nanoparticles and irradiating animals with laser light (180 J/cm²).

As expected, the PDT treatment with Methylene Blue free dye did not affect the tumor growth when compared to the control group. This is attributed to the well-known ability of blood enzymes to reduce free Methylene Blue to the photo chemically-inactive form of Leuko-Methylene Blue, resulting in the loss of photodynamic activity [39].

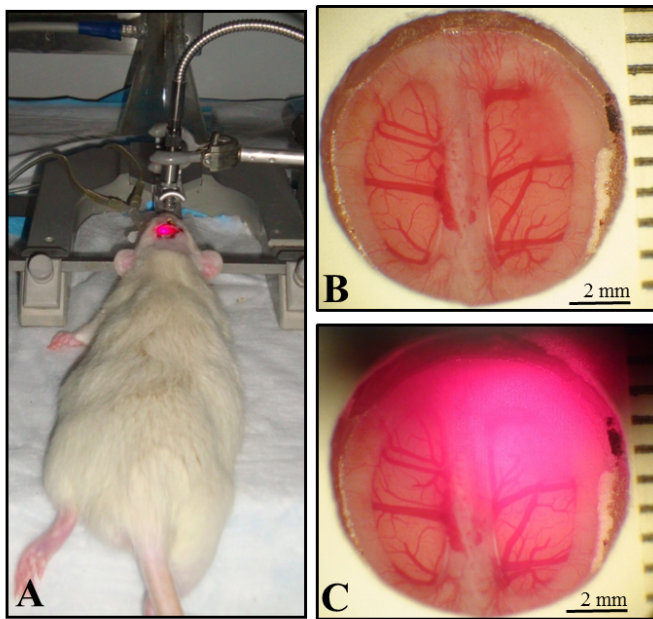


Figure 8: (A) Photograph displaying therapy setup. Rats with BTW are positioned in stereotaxic frames with distance between cranial window and laser collimator fixed at 1 inch. Photographs of a tumor as seen through the BTW (B) before exposure and (C) during irradiation with a 671 nm laser.

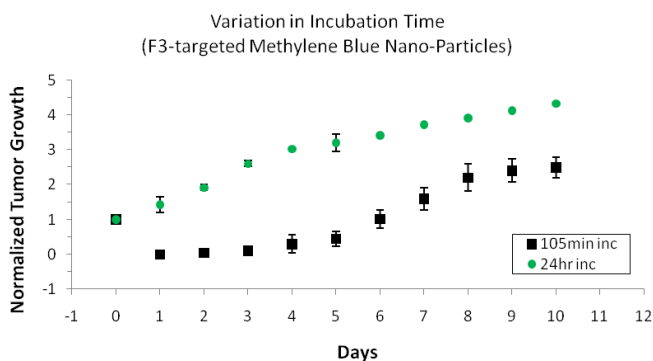


Figure 9: Incubation time dependent effects of photodynamic therapy treatment. F3-targeted Methylene Blue polyacrylamide nanoparticles were intravenously injected, and once completing 105 minutes or 24 hours of systemic incubation, the tumors were irradiated at 180 J/cm² through the BTW and observed daily.

Overall there were significant statistical differences in median tumor size between the control and Methylene Blue free dye treatment, versus that by Methylene Blue polyacrylamide nanoparticles, whether F3-targeted or non-targeted (Figure 11). When treating the tumors with Methylene Blue polyacrylamide nanoparticles there is a significant arrest of tumor growth. However, the insignificant differences between the two delivery methods, of F3-targeted and PEGylated *versus* PEGylated NPs, indicates that the use of F3-peptide did not significantly improve the PDT outcome. The similar growth trends of the targeted and non-targeted PEG polyacrylamide nanoparticles imply that the nanoparticles effectively accumulated in the tumor sites via passive targeting, involving EPR; this is consistent with our previous MRI based findings, that active targeting improves the uptake of such nanoparticles in rat models of 9 L glioma only for circulation times longer than 2 hrs [40]. On the other side, these results clearly demonstrate the advantages of NP-based PDT agents, due

to targeting (passive or active), as well as due to protection of the photo drug from degradation by blood enzymes. In a forthcoming publication we study a similar system, where the effects of enzyme degradation are negligible, so as to separate this effect from the NP targeting advantage. We also notice that the tumor growth was retarded for a period of time but continued to progress for all groups, including the animals treated with PEGylated Methylene Blue polyacrylamide nanoparticles. This is probably because the tumor was illuminated from only one direction, i.e. through the cranial window, due to constraints imposed by the BTW. However in a clinical setting, where light can be directed at all angles for intra-operative PDT, we believe that this illumination problem can be overcome, resulting in a significantly higher efficacy.

We also note that the choice of 105 min time period between injection and PDT treatment was based on our knowledge that at that time there were equal amounts of targeted and non-targeted NPs [53]. After that time, the tumor tissue concentration of the former increases while that of the latter decreases [40]. Thus we believe that choosing a later or longer period for illumination may have significantly improved the relative efficacy for the targeted NPs.

To deal with our results on tumor necrosis, we emphasize that tumor growth patterns were calculated by measuring the surface area of the tumor tissue as seen through the BTW. Notably, the subsequent outcome of treatment proves important in the evaluation of treatment success.

Figures 12 and 13 compares the surface area measurements of necrotic tissue for F3-targeted and non-targeted Methylene Blue polyacrylamide nanoparticles. The day of treatment and one day post-treatment showed no detectable traces of necrosis, however outstanding amounts of necrotic tissue appeared two days post-treatment and dissipated through day six as the necrotic tissue was no longer visible due to microglia and astrocytes (glial cells) removing the damaged tissue in addition to tumor tissue regrowth.

Optical penetration depth in tissue is the distance through which the radiant power decreases to 1/e or 37% of its initial value [61]. Beyond this depth, tissue is exposed to laser light of a lower intensity, which still may be adequate for PDT. Methylene Blue dye has a long absorption wavelength ($\lambda_{max} = 670 \text{ nm}$) allowing for good penetration depth of laser light in live tissues, however the penetration of light through the tumor is dependent on the characteristics of the treated tissue. Laser light at 631 nm can achieve a penetration depth of $1.5 \pm 0.43 \text{ mm}$ in brain tissue and $2.9 \pm 1.5 \text{ mm}$ in brain tumor tissue [62]. The rat models used in these experiments contained tumor implants extending into the cortex, a depth which may exceed the penetration depth achievable by our 671 nm laser. This limitation resulted in incomplete eradication of the base of the tumor, resulting in detectable growth patterns days after treatment. However, PDT is still expected to be effectively applied as a post-surgical adjunctive treatment because there the microscopic residual tumor tissue is within effective range.

Conclusions

This work demonstrates effective eradication of 9L glioma cells, using photo-active nanoparticles (NPs). These nanoparticles encapsulate the Methylene Blue (MB) photosensitizer in a spherical hydrogel matrix with a mean diameter of 55 nm, containing approximately 0.27% dye by weight. Such photosensitive nanoparticles prove suitable for the eradication of 9L glioma both *in vitro* and *in vivo*. *In vivo* visual observations through the BTW (brain tumor window) allow a serial inspection of efficacy of various treatment protocols, investigating photosensitizer delivery and incubation time (time between nanoparticle administration and laser treatment). Quantitative tumorigenic responses and growth patterns presented a more favorable treatment outcome for animals receiving treatment 105

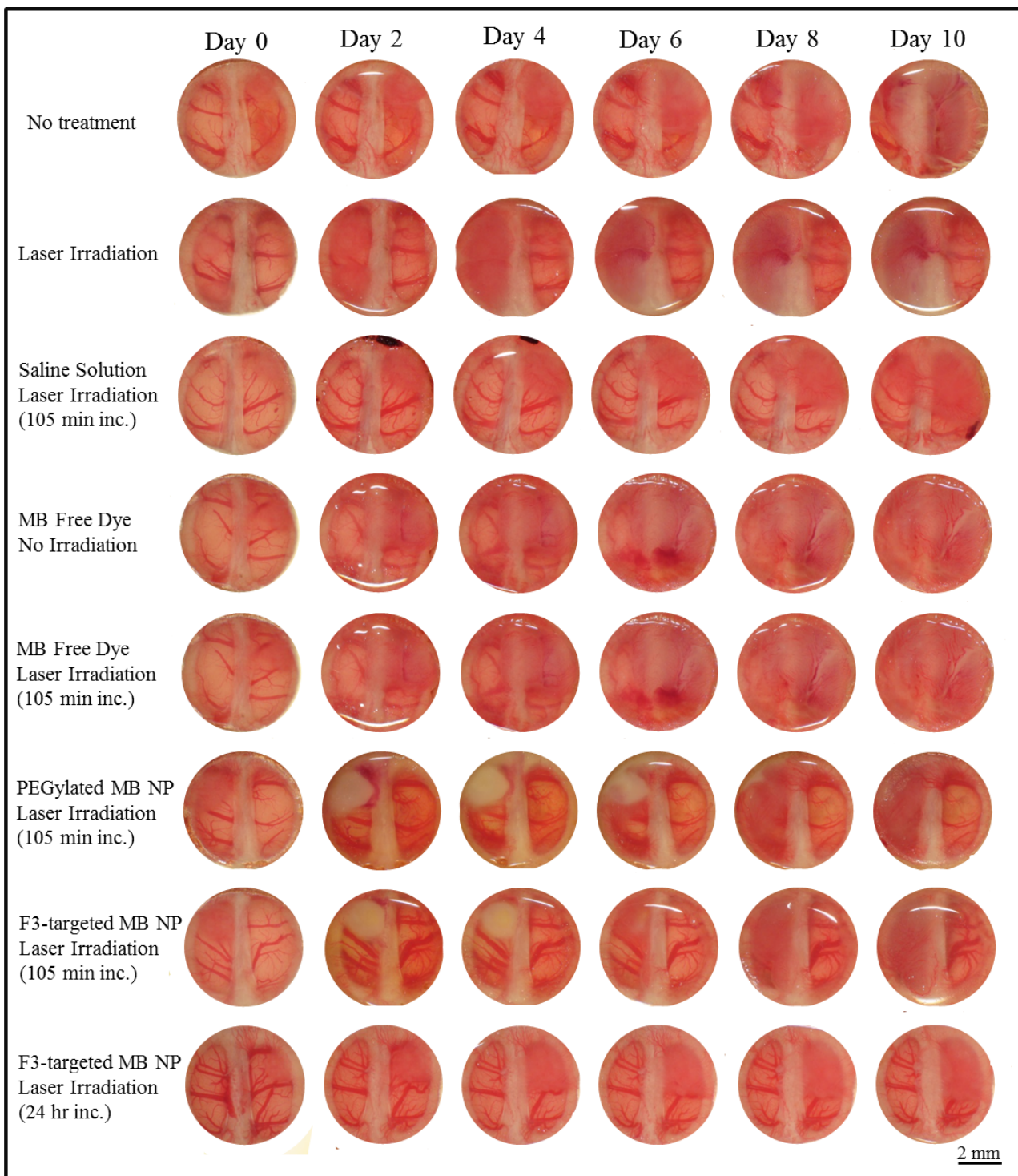


Figure 10: Daily photographs of the cortical surface depict tumor growth, images taken through brain tumor windows on rat models. Animal groups receiving irradiation experienced a fluence dose of 180 J/cm^2 using a 671 nm laser. Note that with the use of free MB dye (no NP's) laser irradiation does not make a difference (because the MB dye was turned into Leuko MB by the body's enzymes)

minutes after nanoparticle administration, compared to animals with a 24 hour incubation time. When investigating photosensitizer delivery methods, the injection of unencapsulated Methylene Blue shows no effect in the reduction/necrosis of tumor mass; in contrast, both the targeted and non-targeted Methylene Blue nanoparticles resulted in tumor necrosis development and significant delays in tumor progression post-treatment. When tested under the condition of equal NP tumor

content and MB loading, the targeted and untargeted NPs showed comparable efficacy. However, we note that under such equal dose and delivery conditions, we expect the targeted NPs to have a superior therapeutic index, which was not tested. With the demonstrated substantial improvements in tumor response to treatment, over control groups, such as naked MB dye, the nanoparticle-based PDT agents prove advantageous for the eradication of local tumors.

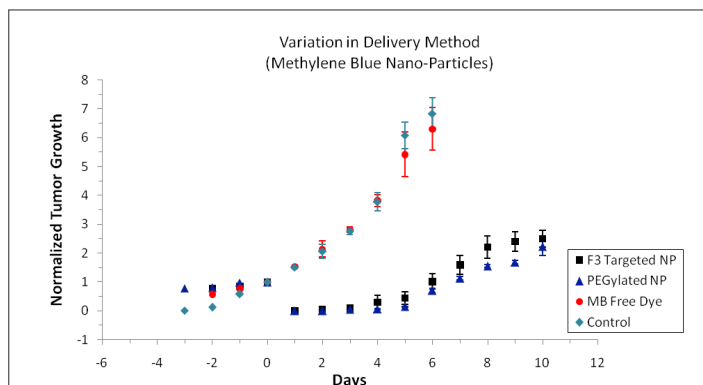


Figure 11: Effect of PDT treatment delivered 105 minutes after injection of Methylene Blue F3-targeted nanoparticles, Methylene Blue PEGylated nanoparticles and Methylene Blue free dye. The control animal was not administered with photosensitizer or exposed to the laser illumination. Another control animal group treated with light illumination showed the same tumor growth trend as the “no treatment” control animal group

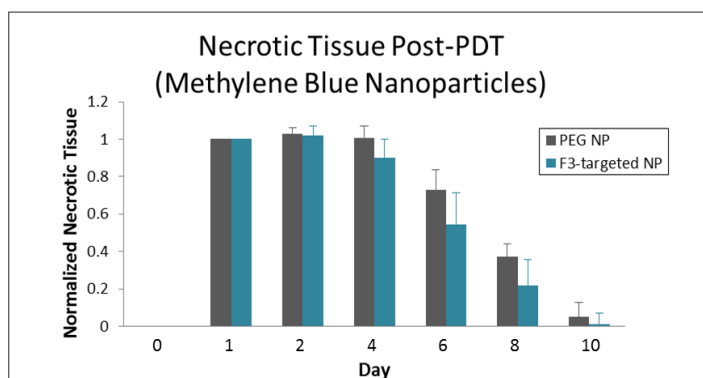


Figure 12: Post-PDT treatment necrotic tissue measurements for tumors treated with F3-targeted Methylene Blue polyacrylamide nanoparticles versus non-targeted (PEGylated) Methylene Blue nanoparticles. Both treatment groups express similar necrotic formation and regression patterns with a greater formation of necrotic tissue for non-targeted Methylene Blue nanoparticles

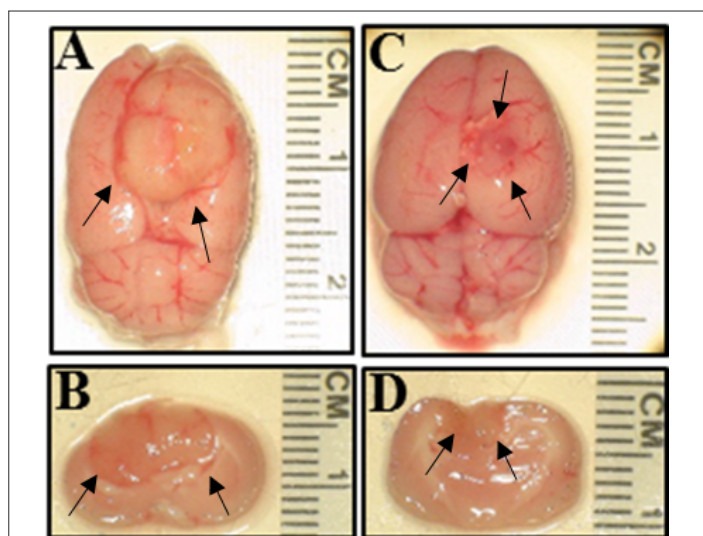


Figure 13: Gross specimen from animal model, excised 10 days post-PDT therapy. Representation of brain tumor for animal groups (A,B) without photosensitizer or laser illumination, and (C,D) animals receiving non-targeted Methylene Blue nanoparticles (105 minute incubation time) with irradiation fluence dose of 180 J/cm² using a 671 nm laser

Finally it is of note that such photo-reactive nanoparticles have the potential to be used for photodynamic therapy as well as for delineating neurosurgery. Such targeted, blue dye loaded, nanoparticles, administered prior to surgery, would help first to delineate tumor boundaries and then, after maximal resection, to eradicate residual tumor tissue, thereby minimizing the need for post-surgical adjuvant therapy. This novel approach of combined delineated surgery and intra-operative photodynamic-therapy constitutes a potential breakthrough for the treatment of glioma.

Acknowledgement

We acknowledge funding support from the University of Michigan Rackham Graduate School Merit Fellowship (KAL) and the NIH/NIBIB “quantum” grant R01EB007977 (RK,OS,MP).

References

- Alifieris C, Trafalis DT (2015) Glioblastoma multiforme: Pathogenesis and treatment. *Pharmacol Ther* 152: 63-82.
- Stupp R, Mason WP, van den Bent MJ, Weller M, Fisher B, et al. (2005) Radiotherapy plus concomitant and adjuvant temozolomide for glioblastoma. *N Engl J Med* 352: 987-96.
- Westphal M, Hilt DC, Bortey E, Delavault P, Olivares R, et al. (2003) A phase 3 trial of local chemotherapy with biodegradable carmustine (BCNU) wafers (Gliadel wafers) in patients with primary malignant glioma. *Neuro Oncol* 5: 79-88.
- Sharman WM, Allen CM, van Lier JE (1999) Photodynamic therapeutics: basic principles and clinical applications. *Drug Discov Today* 4: 507-517.
- Pushpan SK, Venkatraman S, Anand VG, Sankar J, Parmeswaran D, et al. (2002) Porphyrins in photodynamic therapy—a search for ideal photosensitizers. *Curr Med Chem Anticancer Agents* 2: 187-207.
- Mellish KJ, Cox RD, Vernon DI, Griffiths J, Brown SB (2002) In Vitro Photodynamic Activity of a Series of Methylene Blue Analogues. *Photochem Photobiol* 75: 392-397.
- Orth K, Rück A, Stanescu A, Beger HG (1995) Intraluminal treatment of inoperable oesophageal tumours by intralesional photodynamic therapy with methylene blue. *Lancet* 345: 519-520.
- DeRosa MC, Crutchley RJ (2002) Photosensitized singlet oxygen and its applications. *Coordination Chemistry Reviews* 233: 351-371.
- Hopper C (2000) Photodynamic therapy: a clinical reality in the treatment of cancer. *Lancet Oncol* 1: 212-219.
- Redmond RW, Gamlin JN (1999) A compilation of singlet oxygen yields from biologically relevant molecules. *Photochem Photobiol* 70: 391-475.
- Severino D, Junqueira HC, Gugliotti M, Gabrielli DS, Baptista MS (2003) Influence of Negatively Charged Interfaces on the Ground and Excited State Properties of Methylene Blue. *Photochem Photobiol* 77: 459-468.
- Junqueira HC, Severino D, Dias LG, Gugliottia MS, Baptist MS (2002) Modulation of methylene blue photochemical properties based on adsorption at aqueous micelle interfaces. *Phys Chem Chem Phys* 4: 2320-2328.
- Eimer MT, Kelly JM (1993) New trends in photobiology: photochemical interactions of methylene blue and analogues with DNA and other biological substrates. *J Photochem Photobiol B* 21: 103-124.
- Ball DJ, Luo Y, Kessel D, Griffiths J, Brown SB, et al. (1998) The induction of apoptosis by a positively charged methylene blue derivative. *J Photochem Photobiol B* 42: 159-163.
- Wainwright M, Phoenix DA, Rice L, Burrow SM, Waring J (1997) Increased cytotoxicity and phototoxicity in the methylene blue series via chromophore methylation. *J Photochem Photobiol B* 40: 233-239.

16. Jockusch S, Lee D, Turro NJ, Leonard EF (1996) Photo-induced inactivation of viruses: adsorption of methylene blue, thionine, and thiopyronine on Qbetabacteriophage. *Proc Natl Acad Sci USA* 93: 7446-7451.
17. Mark W (1996) Non-porphyrin photosensitizers in biomedicine. *Chem Soc Rev* 25: 351-359.
18. Wainwright M, Crossley KB (2002) Methylene blue-a therapeutic dye for all seasons? *J chemother* 14: 431-443.
19. Brooks MM (1936) Methylene blue as an antidote for cyanide and carbon monoxide poisoning. *The Scientific Monthly* 43: 585-586.
20. Schirmer RH, Coulibaly B, Stich A, Scheiwein M, Merkle H, et al. (2003) Methylene blue as an antimalarial agent. *Redox report* 8: 272-275.
21. Guttman P, Ehrlich P (1891) Über die Wirkung des Methylenblau bei Malaria" (On the effect of methylene blue on malaria). *Berliner Klinische Wochenschrift*, 28: 953-956.
22. Medina DX, Caccamo A, Oddo S (2011) Methylene blue reduces $\alpha\beta$ levels and rescues early cognitive deficit by increasing proteasome activity. *Brain Pathol* 21: 140-149.
23. Wischik CM, Edwards PC, Lai RY, Roth M, Harrington CR (1996) Selective inhibition of Alzheimer disease-like tau aggregation by phenothiazines. *Proceedings of the National Academy of Sciences Proc Natl Acad Sci USA* 93: 11213-11218.
24. Bellin JS, Mohos SC, Oster G (1961) Dye-sensitized photoinactivation of tumor cells in vitro. *Cancer Res* 21: 1365-1371.
25. Orth K, Beck G, Genze F, Rück A (2000) Methylene blue mediated photodynamic therapy in experimental colorectal tumors in mice. *J Photochem Photobiol B* 57: 186-192.
26. Williams JL, Stamp J, Devonshire R, Fowler GJ (1989) Methylene blue and the photodynamic therapy of superficial bladder cancer." *J Photochem Photobiol B* 4: 229-232.
27. Orth K, Russ D, Beck G, Rück A, Beger HG (1998) Photochemotherapy of experimental colonic tumours with intra-tumorally applied methylene blue. *Langenbecks Arch Surg* 383: 276-281.
28. Dalla Via L, Marciani Magno S (2001) Photochemotherapy in the treatment of cancer. *Curr Med Chem* 8: 1405-1418.
29. Tardivo JP, Del Giglio A, Paschoal LH, Ito AS, Baptista MS (2004) Treatment of melanoma lesions using methylene blue and RL50 light source. *Photodiagnosis Photodyn Ther* 1: 345-346.
30. Tardivo JP, Del Giglio A, Paschoal LH, Baptista MS (2006) New photodynamic therapy protocol to treat AIDS-related Kaposi's sarcoma. *Photomed Laser Surg* 24: 528-531.
31. Photodynamic Therapy Associated with Full-mouth Ultrasonic Debridement in the Treatment of Severe Chronic Periodontitis. (2013) In *ClinicalTrials.gov Internet*: Bethesda (MD): National Library of Medicine (US); Escola Bahiana de Medicina e Saude Publica.
32. Gabrieli D (2004) Methylene blue aggregation in liver mouse mitochondria. *Photochem Photobiol* 79: 227-32.
33. Leonard KA, Nelen MI, Simard TP, Davies SR, Gollnick SO, et al. (1999) Synthesis and evaluation of chalcogenopyrylium dyes as potential sensitizers for the photodynamic therapy of cancer. *J Med Chem* 42: 3953-3964.
34. Yao J, Zhang GJ (1996) Loss of lysosomal integrity caused by the decrease of proton translocation in methylene blue-mediated photosensitization. *Biochim Biophys Acta* 1284: 35-40.
35. Zhang LZ, Tang GQ (2004) The binding properties of photosensitizer methylene blue to herring sperm DNA: a spectroscopic study. *J Photochem Photobiol B* 74: 119-125.
36. May JM, Qu ZC, Cobb CE (2004) Reduction and uptake of methylene blue by human erythrocytes. *Am J Physiol Cell Physiol* 286: C1390-C1398.
37. Bongard RD, Merker MP, Shundo R, Okamoto Y, Roerig DL, et al. (1995) Reduction of thiazine dyes by bovine pulmonary arterial endothelial cells in culture. *Am J Physiol* 269: L78-L84.
38. Merker MP, Bongard RD, Linehan JH, Okamoto Y, Vyprachticky D, et al. (1997) Pulmonary endothelial thiazine uptake: separation of cell surface reduction from intracellular reoxidation. *Am J Physiol* 272: L673-L680.
39. Hah HJ, Kim G, Lee YE, Orringer DA, Sagher O, et al. (2011) Methylene Blue-Conjugated Hydrogel Nanoparticles and Tumor-Cell Targeted Photodynamic Therapy. *Macromol Biosci* 11: 90-99.
40. Moffat BA, Reddy GR, McConville P, Hall DE, Chenevert TL, et al. (2003) A novel polyacrylamide magnetic nanoparticle contrast agent for molecular imaging using MRI. *Mol Imaging* 2: 324-332.
41. Weissleder R, Heautot JF, Schaffer BK, Nossiff N, Papisov MI, et al. (1994) MR lymphography: study of a high-efficiency lymphotropic agent. *Radiology* 191: 225-230.
42. Moghimi SM, Hunter AC, Murray JC (2001) Long-circulating and target-specific nanoparticles: theory to practice. *Pharmacol Rev* 53: 283-318.
43. Moghimi SM, Bonnemain B (1999) Subcutaneous and intravenous delivery of diagnostic agents to the lymphatic system: applications in lymphoscintigraphy and indirect lymphography. *Adv Drug Deliv Rev* 37: 295-312.
44. Maeda H, Wu J, Sawa T, Matsumura Y, Hori K (2000) Tumor vascular permeability and the EPR effect in macromolecular therapeutics: a review. *J Control Release* 65: 271-284.
45. Matsumura Y, Maeda H (1986) A new concept for macromolecular therapeutics in cancer chemotherapy: mechanism of tumoritropic accumulation of proteins and the antitumor agent smancs. *Cancer Res* 46: 6387-6392.
46. Maeda H (2001) The enhanced permeability and retention (EPR) effect in tumor vasculature: the key role of tumor-selective macromolecular drug targeting. *Adv Enzyme Regul* 41: 189-207.
47. Barbara WH, Dougherty TJ (1992) How does photodynamic therapy work? *Photochem Photobiol* 55: 145-157.
48. Koo YE, Reddy GR, Bhojani M, Schneider R, Philbert MA, et al. (2006) Brain cancer diagnosis and therapy with nanoplateforms. *Adv Drug Deliv Rev* 58: 1556-1577.
49. Reddy GR, Bhojani MS, McConville P, Moody J, Moffat BA, et al. (2006) Vascular targeted nanoparticles for imaging and treatment of brain tumors. *Clin Cancer Res* 12: 6677-6686.
50. Moreno MJ, Monson E, Reddy RG, Rehemtulla A, Ross BD, et al. (2003) Production of Singlet Oxygen by Ru(dpp(SO₃)₂)₃ Incorporated in Polyacrylamide PEBBLEs. *Sensors and Actuators B: Chemical* 90: 82-89.
51. Yan F, Kopelman R (2003) The Embedding of Meta-tetra (Hydroxyphenyl)-Chlorin into Silica Nanoparticle Platforms for Photodynamic Therapy and Their Singlet Oxygen Production and pH-dependent Optical Properties. *Photochem Photobiol* 78: 587-591.
52. Supporting Your Micro QC Requirements. (2014) *Endotoxin Detection and Microbial Identification*.
53. Orringer DA, Chen T, Huang DL, Armstead WM, Hoff BA, et al. (2010) The brain tumor window model: a combined cranial window and implanted glioma model for evaluating intraoperative contrast agents. *Neurosurgery* 66: 736-743.
54. Vinogradov SV, Bronich TK, Kabanov AV (2002) Nanosized cationic hydrogels for drug delivery: preparation, properties and interactions with cells. *Adv Drug Deliv Rev* 54: 135-147.
55. Mark ED, Shin DM (2008) Nanoparticle therapeutics: an emerging treatment modality for cancer. *Nature Reviews Drug Discovery* 7: 771-782.

56. Maeda H, Bharate GY, Daruwalla J (2009) Polymeric drugs for efficient tumor-targeted drug delivery based on EPR-effect. *Eur J Pharm Biopharm* 71: 409-419.
57. Simmer KA (2014) Improved Efficacy of Localized Brain Tumor Therapy Using Photosensitive Nanoparticles. PhD Thesis, University of Michigan.
58. Moan J, Berg K (1991) The photodegradation of porphyrins in cells can be used to estimate the lifetime of singlet oxygen. *Photochem Photobiol* 53: 549-553.
59. Nie G, Hah HJ, Kim G, Lee YE, Qin M, et al. (2012) Hydrogel nanoparticles with covalently linked coomassie blue for brain tumor delineation visible to the surgeon. *Small* 8: 884-891.
60. Wang S, Fan W, Kim G, Hah HJ, Lee YE, et al. (2011) Novel methods to incorporate photosensitizers into nanocarriers for cancer treatment by photodynamic therapy. *Lasers Surg Med* 43: 686-695.
61. Dougherty TJ, Weishaupt KR, Boyle DG (1985) Photodynamic sensitizers. *Cancer: Principles and Practice of Oncology* 2: 2272-2279.
62. Muller PJ, Wilson BC (1987) Photodynamic therapy of malignant primary brain tumours: clinical effects, postoperative ICP, and light penetration of the brain. *Photochem Photobiol* 46: 929-935.